MOX-Report No. 46/2022

Impact of pressure guidewire on model-based FFR prediction

Lucca, A.; Fraccarollo, L.; Fossan, F.E.; Braten, A.T.; Pozzi, S.;

Vergara, C.; Muller, L.O.

MOX, Dipartimento di Matematica
Politecnico di Milano, Via Bonardi 9 - 20133 Milano (Italy)

mox-dmat@polimi.it http://mox.polimi.it

Impact of pressure guidewire on model-based FFR prediction

Alessia Lucca[1], Luigi Fraccarollo[2], Fredrik E. Fossan[3], Anders T. Bråten[4], Silvia Pozzi[5], Christian Vergara[6], and Lucas O. Müller[1]

[1]Department of Mathematics, University of Trento, Italy
[2]DICAM, University of Trento, Italy
[3]Department of Structural Engineering, Norwegian University of Science and Technology, Norway
[4]Department of Cardiology, Norwegian University of Science and Technology, Norway
[5]MOX, Department of Matematics, Politecnico di Milano, Italy
[6]LABS, Department of chemistry,materials and chemical engineering ”Giulio Natta”, Politecnico di Milano, Italy

March 2022

1 Abstract

Fractional Flow Reserve (FFR) is used to characterize the functional significance of coronary artery stenoses. FFR is assessed under hyperemic conditions by invasive measurements of trans-stenotic pressure thanks to the insertion of a pressure guidewire across the coronary stenosis during catheterization. In order to overcome the potential risk related to the invasive procedure and to reduce the associated high costs, blood flow simulations that incorporate clinical imaging and patient-specific characteristics have been proposed. Most CCTA-derived FFR models neglect the potential influence of the guidewire on the flow and pressure. We aim to quantify the impact of taking into account the presence of the guidewire in model-based FFR prediction. We adopt a CCTA-derived FFR model and perform simulations with and without the guidewire for 18 patients with suspected stable CAD. Presented results show that the presence of the guidewire leads to a tendency to predict a lower FFR value. The FFR reduction is prominent in cases of severe stenoses, while the influence of the guidewire is less pronounced in cases of moderate stenoses. Particular attention should be drawn to intermediate stenoses, in which the presence of the guidewire can change the diagnostic outcome and consequently the clinical decision.

Keywords: CAD, FFR, pressure guidewire

2 Introduction

Coronary artery disease (CAD) is one of the leading causes of death in the world [24]. CAD is caused by the buildup of atherosclerotic plaques in the coronary vessel wall,

resulting in a reduction in oxygen supply to the heart tissue and possibly leading to cardiovascular-related events such as myocardial infarction and unstable angina [13].

In the clinical setting, both medical imaging techniques and invasive functional assessment procedures are used for the detection of stenoses in coronary arteries and, depending on the characteristics of the atherosclerotic lesions, several alternative treatments are applied [27]. Currently, the gold standard for diagnosis of functional severity of ischemia-inducible coronary stenosis is the Fractional Flow Reserve (FFR) [16]. Clinically, FFR of a given coronary lesion is assessed invasively after administration of a pharmacologial vasodilator agent (i.e. adenosine, papaverine) to induce hyperemia. During transfemoral or transradial catheterization a guiding wire equipped with a miniaturised pressure sensor is inserted into the coronary artery to record simultaneously the pressure in the aorta (p_a) and the pressure approximately 2-3 cm distal to the lesion (p_d) that is to be investigated. FFR is then determinate as a ratio of the mean of p_d and p_a tracings [14]. FFR thresholds are defined in order to guide therapy for stable CAD and to decide whether a surgical procedure is needed or patients can just be treated with optimal medical therapy. Trials evaluating the prognostic impact of the FFR have shown that revascularisation can be safely deferred if FFR is > 0.80, while a lesion is haemodynamically relevant if FFR < 0.75 and then revascularisation is recommended [14]. There exists a gray zone for FFR between 0.75 and 0.8, where sound clinical judgment should balance the final decision. Even though the European Society of Cardiologists recommends the use of FFR to guide therapy for stable CAD [19], FFR remains underused due to associated costs, its invasive nature and the need of trained interventionalists. This underuse has lead the medical community to look into non-invasive screening tools to select patients that will likely have functional significant lesions.

Coronary computed tomography angiography (CCTA) has emerged as a non-invasive method to identify the geometrical significance of a lesion. Studies have shown that it is characterized by high sensitivity and low specificity. Consequently, among CCTA-identified stenoses, only a minority are then found to be functional significant (FFR < 0.8) [2]. Image-based modelling in combination with computational fluid dynamics has proved to be an effective answer to the need of a more selective non-invasive method. This approach allows to predict FFR using only CCTA scans and non-invasive subject-specific clinical data. Fully physics-based models, relying on solving the incompressible Navier-Stokes equations in complex, three-dimensional domains, and also reduced-order models, based on one-dimensional blood flow equations and one-dimensional image processing without the use of supercomputers, have shown a high diagnostic performance [12], [11], [17]. CCTA-derived FFR has proved to complement the anatomical information provided by CCTA to aid diagnosis and reduce the number of unnecessary invasive procedures conducted in patients who turn out to have non-flow-limiting coronary artery stenosis.

Although the presence of the guidewire is often neglected, studies conducted both in vitro [10] and computationally with idealized geometries and in a patient-specific domain [21] have shown that the haemodynamic alteration caused by the presence of the guidewire, can lead to an underestimation of the FFR predicted by the clinical invasive measure.

The goal of this article is to quantify the impact of considering the presence of the pressure guidewire in FFR prediction for a wide range of FFR values and considering several patients. After adopting a CCTA-derived FFR model, we performed three-

dimensional computer simulations in the configuration with and without the presence of the pressure guidewire on a sample of 18 patients with suspected stable CAD. Flow rates, pressure distributions and predicted FFR in both configurations were then analyzed and compared.

3 Materials and Methods

3.1 Patient Population

We consider a population of 18 patients recruited as part of a clinical trial at St. Olavs hospital, Trondheim, Norway [4]. The subjects included in this study had undergone invasive angiography with FFR measurements after CCTA recommendations. The exlcusion criteria applied during the recruitment phase were the followoing: unstable coronary artery disease; previous percutaneous coronary intervention or bypass surgery; renal insufficiency; contraindication to use of vasodilator agents and non diagnostic quality of the CCTA.

The patients presented at least one suspected lesion, resulting in a collection of 24 FFR measurements. Patients were selected from a larger patient pool in order to obtain a homogeneous distribution of invasive FFR values. Tables 1 and 2 provide an overview of general patient characteristics and invasive FFR measurements.

Patient IDs	MAP(mmHg)	CO (L min^{-1})	Dominance
1	93.33	6.0	right
2	95.67	3.8	right
3	92.67	6.2	right
4	97.67	6.5	right
5	84.33	4.4	right
6	99.33	5.2	right
7	95.33	3.6	right
8	100.33	6.3	left
9	98.67	3.4	right
10	100.67	5.4	left
11	115.33	6.4	right
12	92.33	4.9	right
13	88.67	6	right
14	99.33	3.97	right
15	90.0	4.3	right
16	105.33	4.66	right
17	99.0	3.88	right
18	100.0	5.25	right

Table 1: Patient-specific data for the 18 patients considered in this work. MAP (mean aortic pressure), CO (cardiac output) and dominance are reported.

FFR IDs	Patient IDs	Lesion location	FFR
1	1	mLAD	0.68
2	2	mLAD	0.52
3	2	dLAD	0.46
4	2	pLCX	0.88
5	3	mLAD	0.87
6	4	pLAD	0.5
7	4	2^{nd} diagonalLAD	0.51
8	5	LCX	0.71
9	6	pLAD	0.6
10	7	mLAD	0.59
11	8	LCX	0.38
12	9	mLAD	0.92
13	10	pRCA	0.74
14	11	pLAD	0.7
15	12	mLAD	0.8
16	13	mLAD	0.77
17	13	LCX	0.72
18	14	mRCA	0.96
19	15	mLAD	0.44
20	16	mLAD	0.78
21	16	LCX	0.52
22	17	mLAD	0.83
23	17	1^{st} diagonalLAD	0.89
24	18	dRCA	0.84

Table 2: Data for invasive FFR measurements. Location of the lesion and FFR clinically measured are reported. Prefixes p, m, d represent the proximal, the mid and the distal tract of the coronary artery to which they are related. Nomenclature according to [20].

3.2 Data Collection and Processing

3.2.1 Medical Data Acquisition

CCTA was performed using two CT scanners with 2×128 detector rows (Siemens dual source Definition Flash) following a standardized protocol.

FFR was measured using Verrata Plus (Philips Volcano, San Diego, USA) pressure wires according to standard practice. Prior to inserting the pressure wire into the coronary artery, intracoronary nitroglycerin was administered and hyperemia was induced by continuous intravenous infusion of adenosine. Pressure and ratio p_d/p_a were recorded over several cycles and FFR was taken equal to the lowest observed value of the ratio.

Standard non-invasive diastolic and systolic pressure measurements were performed on both arms as a part of clinical routine, while cardiac output (CO) was calculated on the basis of the cross-sectional area of the left ventricle outflow tract and velocity time integral derived from Pulse Wave Doppler.

3.2.2 Coronary Vessel Segmentation and Volume Meshing

Starting from the CCTA scan, the geometry representing the vascular lumen of the coronary tracts of interest was segmented using the open-source software ITK-SNAP [3]. Surface mesh processing, addition of flow extensions and 3D meshing was performed using the open-source library Vascular Modeling ToolKit [22], leading to the anatomical model.

To investigate the influence of the physical presence of a pressure wire in the clinical measurements of FFR, it is necessary to reproduce the fluid dynamic situation also in its presence. The guidewire was modelled as a curvilinear tube of given diameter (0.036 cm, according to the diameter of the pressure guidewire used in the clinical setting), created starting from the centerline of the stenotic branch. Its presence in the stenotic branch was reproduced by performing a Boolean difference between the mere anatomical model and the tube representing the catheter inserted axially into the stenotic vessel, using the software Blender [7]. The last step involved the meshing process performed using Gmsh software [15]. A schematic representation of the meshing process for the insertion of the pressure guidewire into the stenotic branch is reported in Figure 1.

3.3 Computational Model for Blood Dynamic

Although some works considered compliant vessels for numerical simulations in stenotic coronaries (see e.g. [6, 5]), in this work the segmented coronary tree was considered as rigid domain, whose boundary was decomposed into the inlet section, the surface delimiting the vessel lumen jointly with the interface between the surface of the wire and the blood and N outlets sections, depending on the patient. We assumed the flow regime to be laminar and the blood was modelled as a homogeneous incompressible Newtonian fluid with density 1.05 g cm^{-3} and viscosity 0.035 g cm^{-1} s^{-1}.Then, to describe its fluid dynamic behaviour Navier-Stokes equations for incompressible flows supplemented with the initial status of the fluid velocity and with boundary conditions were discretize both in space and time and were numerically solved. The numerical

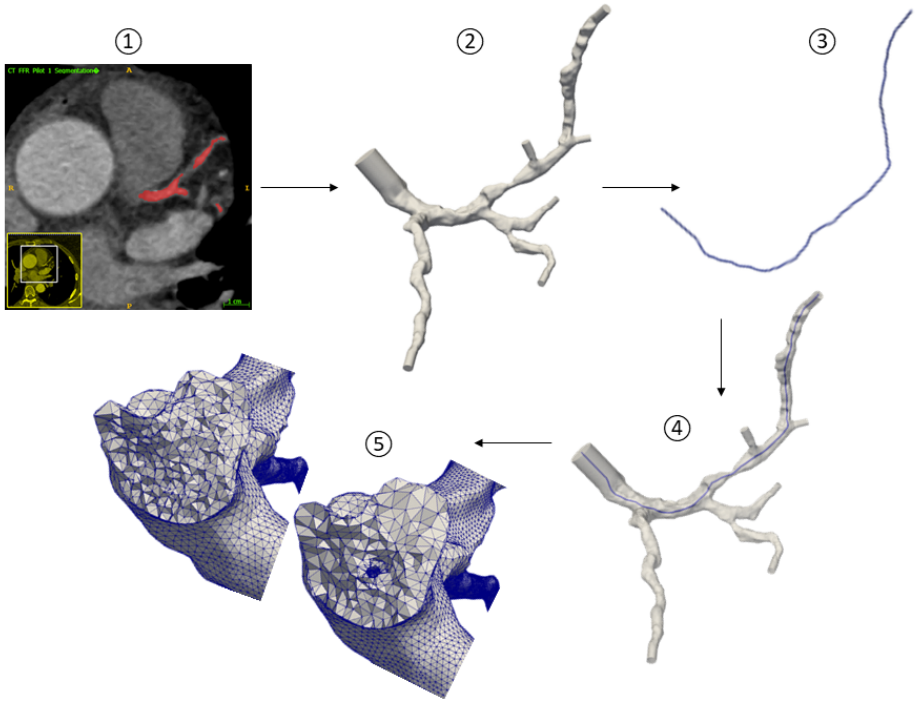

Figure 1: Illustration of the segmentation and meshing process: (1) coronary artery segmentation, (2) preparation of computational domain, (3) guidewire creating from stenotic branch centerline, (4) Boolean difference between the mere coronary tree and the tube, (5) sections of both meshes: with and without the guidewire.

scheme applied is the Incremental Pressure Correction Scheme, described in [8] together with a backward Euler method for time discretizartion. The time step was set to $\Delta t = 1$ms.

In this work we performed simulations considering two different settings, adopting the methodology described in Fossan et al. [12] and Müller et al. [23]. We imposed pressure as inlet boundary condition and, in the first setting (Scenario I), flows at all outlets via prescribed parabolic velocity profile, while in the second setting (Scenario II) we coupled each outlet to a lumped parameter model. The lumped parameter setup, depicted in Figure 2, is derived from the original work by Mantero et al. [25] and represents a Windkessel model composed of three resistances and two compliances, one of which is connected to a pressure source representing the left ventricle pressure. This coupling ensures physiological boundary conditions which take into account the presence of the remaining part of the circulatory system and also the increased impedance experienced by the coronary arteries during the systole. In addition, in both settings a no-slip condition was imposed at the lumen surface and on the interface between the guidewire surface and the blood.

The simulations were performed with FEniCS using CBCFLOW [1]. The computational meshes are composed of tetrahedral elements. The average ratio between a tetrahedral edge length and the radius of the vessel at a given location was set to 0.21 for the wire-absent configuration and to 0.18 for the wire-included configuration resulting in meshes that have on average 985181 elements, (see Figure 1). The discretization is based on finite element methods. It has been used piecewise-quadratic polynomials to approximate the velocity field, while linear polynomials were used for the pressure. A mesh independence study was performed on two geometries with

and without guidewire to verify that the adopted meshing parameter, which in turn defines the mesh elements density, resulted in mesh independent solutions in terms of FFR prediction (relative error respect to solution obtained with the finest mesh below to $1e-2$). See [12] for further details related to the 3D framework.

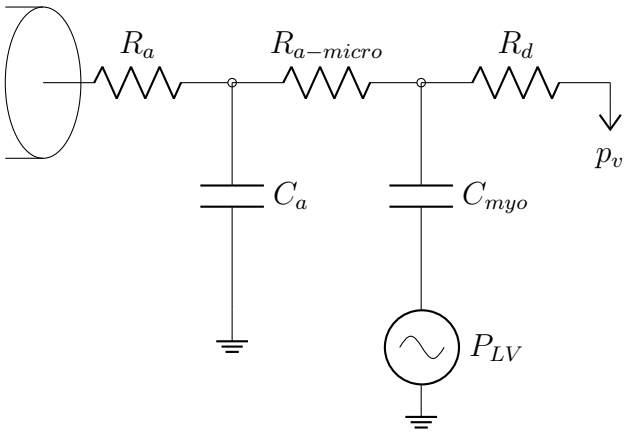

Figure 2: Schematic representation of the coronary bed model coupled to each domain outlet. The coronary bed is embodied by a single arterial path (R_a, C_a, $R_{a-micro}$) and a single venous path represented only by a distal resistance R_d. The two paths are connected by the myocardial compliance C_{myo} which is affected by the time-varying left ventricular pressure P_{LV} [12].

3.4 FFR prediction modelling pipeline

The approach for non-invasive FFR prediction presented in this study follows the modelling pipeline first introduced by Müller et al. [23]. We computed a baseline state using clinical data according to Scenario I, then based on the resulting distribution of pressure and flow, a hyperemic state was predicted under Scenario II.

The modelling pipeline consists of the following steps:

1. define total baseline flow that enters the coronary tree;
2. distribute the flow among the N outlets according to one among several flow distribution criteria available in the literature [23];
3. perform a baseline steady state simulation with prescribed inlet pressure and prescribed outlet flows (Scenario I);
4. compute baseline peripheral coronary resistances according to the pressure and flow distribution of the resting simulation

$$R^{bln}_{out,k} = \frac{p^{bln}_{out,k} - p_v}{q^{bln}_{out,k}} \; k = 1, \ldots, N \tag{1}$$

where $p^{bln}_{out,k}$ and $q^{bln}_{out,k}$ are the pressure and flow at $k-th$ outlet resulted from the baseline simulation performed in Step 3 and p_v is a reference venous pressure set to $p_v = 5$ mmHg;

5. compute hyperemic peripheral coronary resistances

$$R_{out,k}^{hyp} = \frac{R_{out,k}^{bln}}{TCRI} \; k = 1, \ldots, N \tag{2}$$

where Total Coronary Resistance Index (TCRI) is a hyperemic factor to account for the effect of drug on peripheral coronary arteries vasodilation required to clinically measure FFR and it is assumed to be $TCRI = 3$ [12];

6. perform a hyperemic transient simulation prescribing at inlet a a properly scaled aortic pressure waveform (normalized curve is reported in Figure 4) and coupling at outlets lumped parameter models with the resistances previously computed (Scenario II);

7. use results from simulation performed in Step 6 to estimate FFR.

There is a variety of methods used in the literature to distribute baseline coronary flow among the coronary vessels [23]. We decided to use two different methods: distal Murray flow distribution and a vessel length-based flow distribution. Distal Murray method assumes a proportionality between the flow and the cube of the outlets' vessel diameters [9], while in the vessel length-based method the flow is distributed among all outlets using a stem-and-crown model, which is based on allometric scaling between the length of coronary arterial tree and the myocardial mass [29],[28]. With Murray's flow setup we refer to hyperemic simulation setting in which peripheral coronary resistances are extracted from baseline simulation's results with the flow distributed according Murray's law, while with vessel length-based flow setup we refer to hyperemic simulation setting in which peripheral coronary resistances are extracted from baseline simulation's results with the flow distributed according the vessel length-based method. See Figure 3 for an overview of the FFR-prediction pipeline.

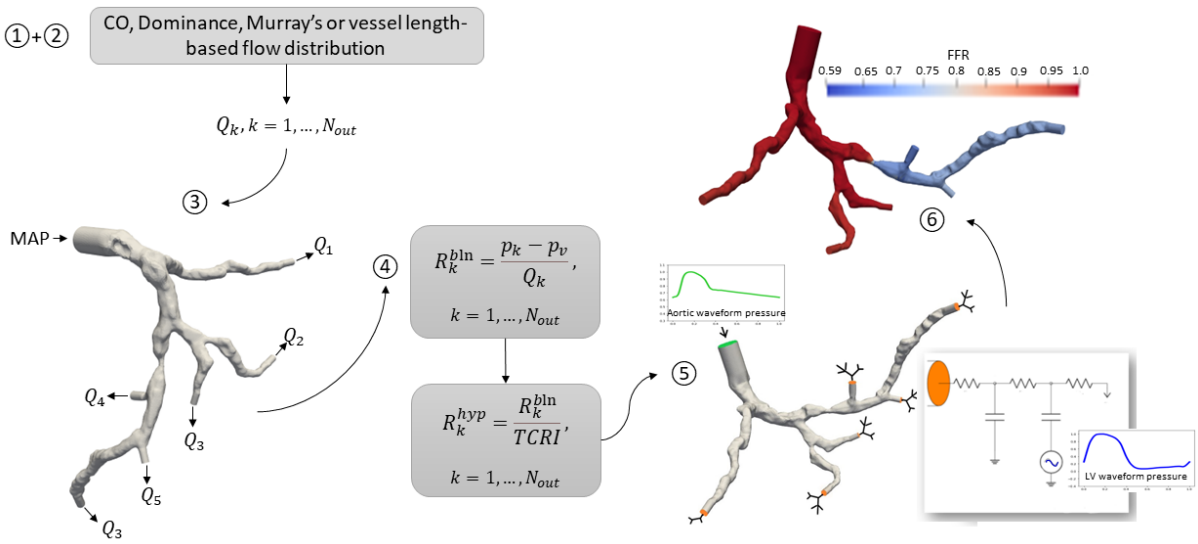

Figure 3: Illustration of the modelling for FFR prediction: (1) + (2) definition of total coronary flow and its distribution among outlets, (3) baseline simulation, (4) compute peripheral coronary resistances based on resting simulation's results, (5) hyperemic simulation, (6) extraction of computational FFR.

3.5 Patient-specific Parameters

The parameters required to perform baseline and hyperemic simulations were extracted from patient-specific clinical data.

For steady state baseline simulations, the mean arterial pressure (MAP) computed as a linear combination of diastolic and systolic blood pressure was prescribed at the inlet of the computational domain, while the total baseline flow to distribute among outlets was assumed to be a portion of the measured CO: $q_{cor} = 0.045$ CO [26] and then distributed according to the selected flow distribution methods.

For transient hyperemic simulations, MAP, pulse pressure and cardiac cycle duration, extracted from clinical tracings, were used to scale the prescribed aortic and left ventricle pressure waveforms, at the inlet section and in lumped parameter models coupled at outlets, respectively. Normalized aortic and left ventricle characteristic waveforms used for patient-specific simulations are shown in Figure 4. Total peripheral compliance was computed as a portion of the arterial compliance of 1.7 mL mmHg^{-1} and then distributed among outlets according to Murray's law. The resulting $C_{out,k}$ and $R^{hyp}_{out,k}$ computed in (2) have to be subsequently distributed among the three different compartments of the Windkessel model coupled to the k-th outlet. The fractions for distributing $R^{hyp}_{out,k}$ among R_a, $R_{a-micro}$, R_d, in relation to Figure 2, are 0.01, 0.84, 0.15, respectively. In the same way $C_{out,k}$ is distributed among C_a and C_{myo} according to fraction 0.025 and 0.975. Parameter distribution among components of lumped-parameter models was taken from [12].

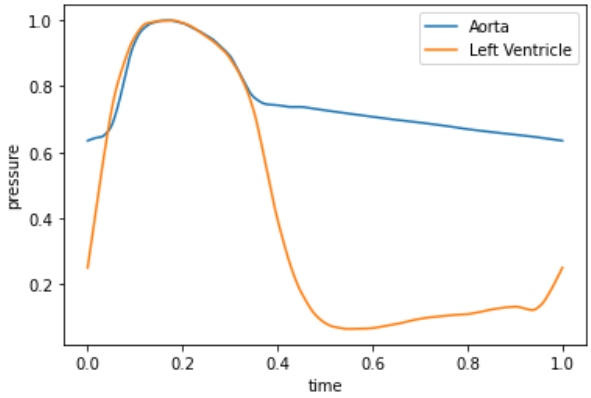

Figure 4: Aortic and left ventricle characteristic waveforms used for patient-specific simulations. Pressure and time are normalized values. The waveform shape are taken from [18].

4 Results

The effects of guidewire insertion on coronary hemodynamics are studied and presented for a population of 18 patients. The 24 FFR measurements collected are distributed among four different ranges of values: 0.38-0.52, 0.52-0.72, 0.72-0.84, 0.84-1. Each FFR range define a class, we refer to class 1 as the group of the most severe stenoses, while class 4 represents the group of the less severe stenoses.

The results are presented in terms of reduction in mean coronary hyperemic flow rate, difference in pressure drop and resulting effect on FFR. The predicted FFR are then evaluated against the invasive FFR clinically measured.

Moreover the resulting pressure distribution and velocity field for some patients are shown in Figure 5.

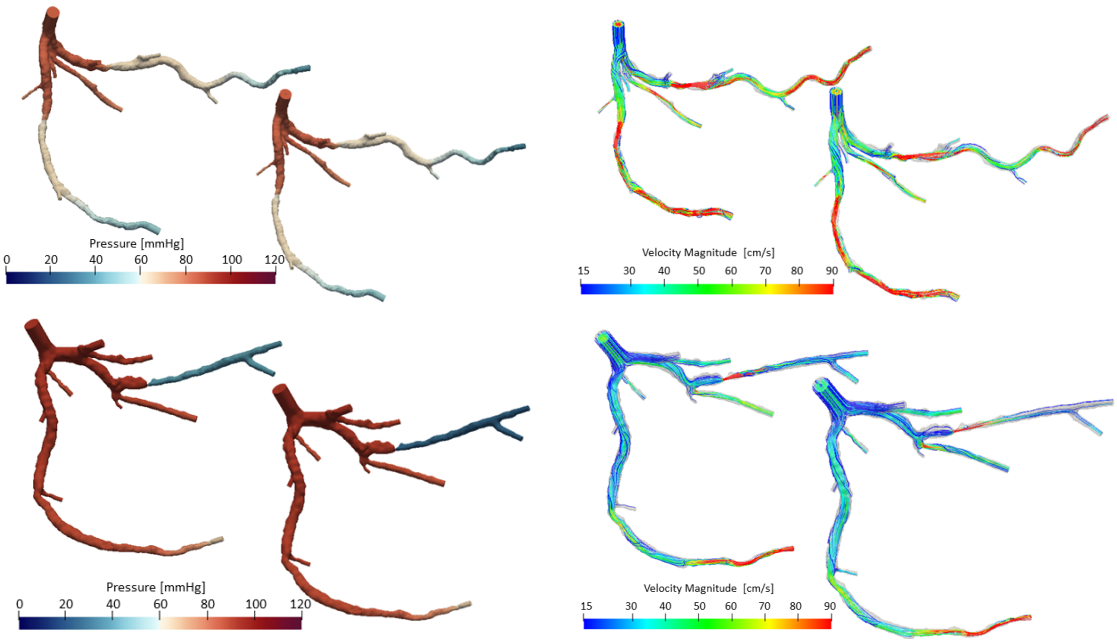

Figure 5: Pressure distribution and velocity field first in the wire-absent configuration and then in the wire-included configuration.

4.1 Guidewire insertion effect on flow discharge

To observe the guidewire flow-obstruction effects, the pulsatile flow rate has been calculated at the inlet section in both conditions: with and without insertion of guidewire into the stenotic branch of each coronary tree. The presence of the pressure guidewire is reflected in a decrease of the mean total flow rate respect to the condition without the guidewire for both flow distribution setups and for all FFR classes. In particular, the average flow reduction observed after the inclusion of the guidewire is of 4.58% for Murray's flow setup and of 6.98% for the vessel length-based flow setup. Average values for each FFR classes are reported in Table 3.

4.2 Guidewire insertion effect on pressure

We computed the trans-stenotic pressure drop after the lesion for both conditions. We observed that a reduction of the lumen contributes to increase the pressure drop and the insertion of the pressure guidewire in the simulations enhances this drop. In the wire-included configuration we noted an average increase of pressure drop of 42.23% across all FFR classes in the Murray's flow setup and of 18.93% using the vessel length-based flow setup.

4.3 Guidewire insertion effect of FFR measurements

FFR is calculated as the ratio of pressure distal to the stenosis p_d computed at the same location where it was clinically measured, to the pressure computed at the ostium of the coronary tree p_a. p_d and p_a are obtained as average values of the cross-sectional pressure over one cardiac cycle. We refer to FFR$_{pred}$ as the computational FFR predicted using the wire-absent condition, while to gFFR$_{pred}$ as the computational FFR predicted using the wire-included condition. Figure 6a compares gFFR$_{pred}$ against FFR$_{pred}$ and shows the FFR$_{pred}$-gFFR$_{pred}$ characteristics for all stenoses under pulsatile hyperemic flow for both flow distribution setups. The difference between FFR$_{pred}$ and gFFR$_{pred}$ increases as the stenosis severity increases. We observed that in the Murray's flow setup the value of predicted gFFR$_{pred}$ decreases on average by 2.2%, 6.7%, 9.4%, 11.7% for class 4, class 3, class 2, class1, respectively. The same trend is recorded also for the predicted gFFR$_{pred}$ with the vessel length-based flow setup. In this configuration, 2.7%, 5.3%, 10.7%, 11.4% are the decrease in FFR for the four ordered class after the inclusion of the wire. The average values are reported in Table 3. Figure 6b compares gFFR$_{pred}$ and FFR$_{pred}$ against the invasive FFR and shows the FFR$_{pred}$-gFFR$_{pred}$ characteristics for all stenoses under pulsatile hyperemic flow for both flow distribution setups. A numerical characterisation of the comparison is given in Table 4.

	Murray's flow setup		
FFR class	drop in FFR	rise in ΔP	drop in inflow
class 4	2.18%	39.06%	3.21%
class 3	6.70%	44.34%	5.94%
class 2	9.40%	47.50%	4.47%
class 1	11.70%	38.00%	4.69%
	vessel length-based flow setup		
FFR class	drop in FFR	rise in ΔP	drop in inflow
class 4	2.71%	19.00%	5.56%
class 3	5.34%	21.84%	5.48%
class 2	10.73%	19.64%	9.94%
class 1	11.38%	15.24%	6.94%

Table 3: For each FFR class here considered we report the mean percentage of predicted FFR drop, increase of trans-stenotic pressure drop and decrease of hyperemic flow rate which we recorded when we move from the wire-absent model to the wire-included model.

5 Discussion

In this study we have presented a framework to perform blood flow simulations for the estimation of FFR based on clinical imaging and patient-specific characteristics with the absence and the presence of a pressure guidewire.

Analysing and comparing the results, we can say that the introduction of the pressure guidewire in CFD simulations can play a significant role. Its presence is associated with an additional pressure loss and a decrease of flow rate, as reported in Table 3. These hemodynamic changes affect the prediction of FFR leading to a tendency

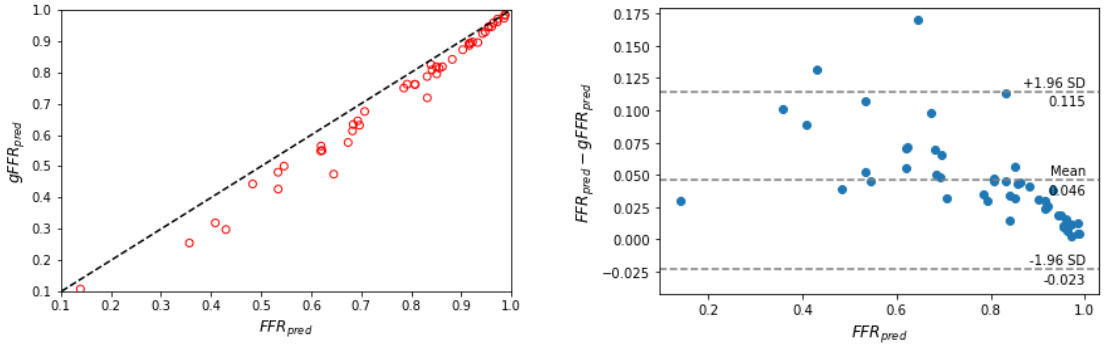

(a)

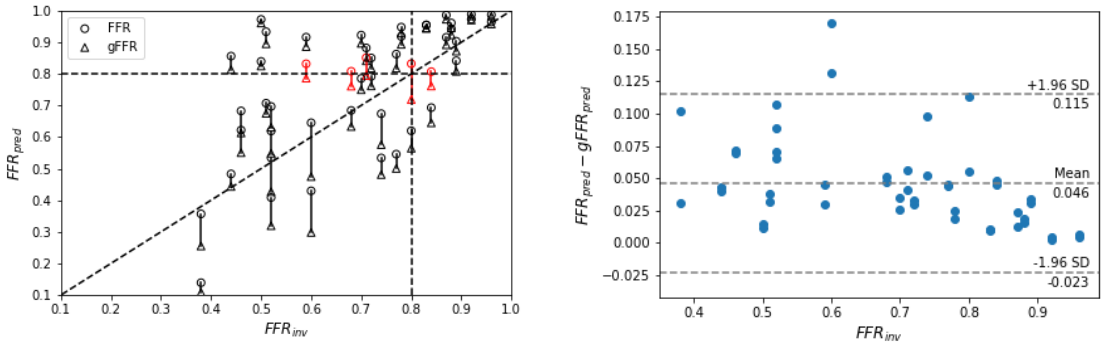

(b)

Figure 6: (a) Comparison of predicted FFR in both models, wire-absent and wire-included model, and for both flow distribution setups and invasive FFR_{inv}. Scatter plot (left) and Bland-Altman plot (right). The scatter plot also highlights (in red) cases which have different classification ($FFR \leq 0.8$) depending on having the guidewire present or not. (b) Comparison of FFR_{pred} and $gFFR_{pred}$ for both flow distribution setups. Scatter plot (left) and Bland-Altman plot (right).

of predicting a lower FFR value. We have observed that the FFR reduction depends on the severity of the stenosis, as it is shown in Figure 6a. Indeed, the difference between the FFR_{pred} and the $gFFR_{pred}$ is less prominent in cases of moderate stenosis, while it is major in more severe cases, where a drop of 11.5% is on averaged recorded compared to an averaged reduction of 2.4% in less severe disease status.

We can conclude that for stenoses with associated FFR included in class 4, class2 or class 1 the impact of the pressure guidewire on stenosis evaluation and clinical decision is of less significance in clinical practise. Indeed, in the first case, the guidewire has negligible effects on predicted FFR, while, on the other hand, the presence of the wire worsens a clinical situation already severe in which the therapy to follow is already evident. The situation is different for intermediate stenoses associated with a FFR included in class 3. In this case the presence of the pressure guidewire could change the diagnosis and a predicted FFR indicating a non-significant ischemia could drop to the ”gray zone” of clinical uncertainty or even suggest a need of surgical intervention when the wire is included in the model, as it is shown in the left plot of Figure 6b.

	Murray's flow setup	
	wire-absent model	wire-included model
Sensitivity	0.35	0.53
Specificity	1.00	0.86
Accuracy	0.54	0.62
Standard deviation	0.14	0.16
Bias	0.13	0.08
AUC	0.84	0.86
	vessel length-based flow setup	
	wire-absent model	wire-included model
Sensitivity	0.76	0.82
Specificity	0.86	0.86
Accuracy	0.79	0.83
Standard deviation	0.17	0.18
Bias	0.03	-0.01
AUC	0.88	0.90

Table 4: Diagnostic index of wire-absent and wire-included model for both flow distribution setup. Sensitivity, specificity and accuracy are described in terms of true positive (TP), true negative (TN), false negative (FN) and false positive (FP) as Sensitivity = TP/(TP+FN), Specificity = TN/(TN+FP), Accuracy = (TN+TP)/(TN+TP+FN+FP). The AUC presents the area under the Receiver Operating Characteristics (ROC) curve plotted by using true positive rate against false positive rate for different cut-points of the diagnostic test.

Table 4 reports the statistics that describe the efficiency of our models as diagnostic tests. We observe that the inclusion of the guidewire in the model leads to a overall improvement of the diagnostic capability of the model balancing accuracy, specificity and sensitivity. In addition, the bias from the clinical measured FFR drops from 0.13 to 0.08 in Murray's law setup and from 0.03 to -0.01 in vessel length-based flow setup when the physical presence of the pressure guidewire is taken into account. In conclusion, our results show that the impact of accounting for the presence of the pressure guidewire in model-based FFR prediction pipelines can play a relevant role, especially

for intermediate and severe stenoses. Including this feature in a modelling pipeline would allow to reduce modelling errors, representing more reliably the clinical setting in which FFR measurements are performed.

5.1 Limitations

The pressure guidewire is assumed to be rigid and static placed axially along the stenotic branch. This represents an ideal situation that not always can be produced in practice since the wire is susceptible to unsteady blood flow. Effects of different positions of the guidewire inside the vessel and a its interaction with the fluid should be investigated. Some modelling hypotheses should be explored. The impact of patient-specific TCRI on FFR prediction should be addressed, as well as different quantification methods of total baseline coronary flow should be investigated. Another limitations is provided by the rigid wall assumption. Although for our application such an assumption could be considered acceptable since the main focus of the paper is to compare two scenarios (with and without guide) both affected by the same limitation, the use of a fluid-structure interaction model could improve the accuracy of the predicted FFR with respect to the invasive one.

References

[1] Logg A., K.A. Mardal, and G. Wells. *Automated solution of differential equations by the finite element method: The FEniCS book*. Vol. 84. Springer Science & Business Media, 2012.

[2] Rossi A., S.L. Papadopoulou, F. Pugliese, B. Russo, A. S. Dharampal, A. Dedic, P.H. Kitslaar, A. Broersen, W.b Meijboom, and R.. van Geuns. “Quantitative computed tomographic coronary angiography: does it predict functionally significant coronary stenoses?” In: *Circulation: Cardiovascular Imaging* 7.1 (2014), pp. 43–51.

[3] Yushkevich P. A., J. Piven, H. C. Hazlett, R. G. Smith, S. Ho, J. C. Gee, and G. Gerig. “User-guided 3D active contour segmentation of anatomical structures: significantly improved efficiency and reliability”. In: *Neuroimage* 31.3 (2006), pp. 1116–1128.

[4] Bråten A.T. and R. Wiseth. *Diagnostic Accuracy of CT-FFR Compared to Invasive Coronary Angiography With Fractional Flow Reserve*. 2017. URL: `ClinicalTrials.gov`.

[5] Guerciotti B., C. Vergara, S. Ippolito, A. Quarteroni, C. Antona, and R. Scrofani. “A computational fluid–structure interaction analysis of coronary Y-grafts”. In: *Medical engineering & physics* 47 (2017), pp. 117–127.

[6] Ramachandra A. B., A. M. Kahn, and A. L. Marsden. “Patient-specific simulations reveal significant differences in mechanical stimuli in venous and arterial coronary grafts”. In: *Journal of cardiovascular translational research* 9.4 (2016), pp. 279–290.

[7] *Blender Foundation*. URL: `www.blender.org`.

[8] Simo J. C. and F. Armero. “Unconditional stability and long-term behavior of transient algorithms for the incompressible Navier-Stokes and Euler equations”. In: *Computer Methods in Applied Mechanics and Engineering* 111.1-2 (1994), pp. 111–154.

[9] Murray C. D. “The physiological principle of minimum work: I. The vascular system and the cost of blood volume”. In: *Proceedings of the national academy of sciences of the united states of america* 12.3 (1926), p. 207.

[10] Ashtekar K. D., L. H. Back, S. F. Khoury, and R. K. Banerjee. “In Vitro Quantification of Guidewire Flow-Obstruction Effect in Model Coronary Stenoses for Interventional Diagnostic Procedure”. In: *Journal of Medical Devices* 1.3 (2007), pp. 185–196.

[11] Fossan F. E., L. O. Müller, J. Sturdy, A. T. Bråten, A. Jørgensen, R. Wiseth, and L. R. Hellevik. “Machine learning augmented reduced-order models for FFR-prediction”. In: *Computer Methods in Applied Mechanics and Engineering* 384 (2021), p. 113892. ISSN: 0045-7825. DOI: https://doi.org/10.1016/j.cma.2021.113892. URL: https://www.sciencedirect.com/science/article/pii/S0045782521002292.

[12] Fossan F. E., J. Sturdy, L. O. Müller, A. Strand, A. T. Bråten, A. Jørgensen, R. Wiseth, and L. R. Hellevik. “Uncertainty quantification and sensitivity analysis for computational FFR estimation in stable coronary artery disease”. In: *Cardiovascular engineering and technology* 9.4 (2018), pp. 597–622.

[13] Neumann F.J., M. Sousa-Uva, A. Ahlsson, F. Alfonso, A.P. Banning, U. Benedetto, R.A.Byrne, J.P. Collet, V. Falk, and S.J. Head. “ESC/EACTS guidelines on myocardial revascularization”. In: *European heart journal* 40 (2018), pp. 87–165.

[14] Sant’Anna F.M. and L.B. Sant’Anna. “Analysis of FFR Measurement Clinical Impact and Cost-Effectiveness Compared to Angiography In Multi-Arterial Patients Undergoing PCI.” In: *Arq Bras Cardiol.* 112.1 (2019), pp. 48–49.

[15] *Gmsh*. URL: www.gmsh.info.

[16] Pijls N. H.J., P. Van Gelder B.and Van der Voort, F. Peels K.and Bracke, H. Bonnier, and M. I. H. El Gamal. “Fractional flow reserve: a useful index to evaluate the influence of an epicardial coronary stenosis on myocardial blood flow”. In: *Circulation* 92.11 (1995), pp. 3183–3193.

[17] Blanco P. J., C. A. Bulant, L. O. Müller, G.D. Talou, C. G. Bezerra, P.A. Lemos, and R. A. Feijóo. “Comparison of 1D and 3D models for the estimation of fractional flow reserve”. In: *Scientific reports* 8.1 (2018), pp. 1–12.

[18] Kim H. J., I. E. Vignon-Clementel, J. S. Coogan, C. A. Figueroa, K. E. Jansen, and C. A. Taylor. “Patient-specific modeling of blood flow and pressure in human coronary arteries”. In: *Annals of biomedical engineering* 38.10 (2010), pp. 3195–3209.

[19] Knuuti J., W. Wijns, A. Saraste, D. Capodanno, E. Barbato, C. Funck-Brentano, E. Prescott, R.F. Storey, C. Deaton, T. Cuisset, S. Agewall, K. Dickstein, T. Edvardsen, J. Escaned, B.J. Gersh, P. Svitil, M. Gilard, D. Hasdai, R. Hatala, F. Mahfoud, J. Masip, C. Muneretto, M. Valgimigli, S. Achenbach, J.J. Bax, and ESC Scientific Document Group. "2019 ESC Guidelines for the diagnosis and management of chronic coronary syndromes: The Task Force for the diagnosis and management of chronic coronary syndromes of the European Society of Cardiology (ESC)". In: *European Heart Journal* 41.3 (2019), pp. 407–477.

[20] Leipsic J., S. Abbara, S. Achenbach, R. Cury, J. P. Earls, G.B. J. Mancini, K. Nieman, G. Pontone, and G. L. Raff. "SCCT guidelines for the interpretation and reporting of coronary CT angiography: a report of the Society of Cardiovascular Computed Tomography Guidelines Committee". In: *Journal of cardiovascular computed tomography* 8.5 (2014), pp. 342–358.

[21] Yi J., F. Tian, A. Simmons A., and T. Barber. "A Computational Analysis of the Influence of a Pressure Wire in Evaluating Coronary Stenosis". In: *Fluids* 6.4 (2021), p. 165.

[22] Antiga L., L. Piccinelli M.and Botti, B. Ene-Iordache, A. Remuzzi, and D. A. Steinman. "An image-based modeling framework for patient-specific computational hemodynamics". In: *Medical & biological engineering & computing* 46.11 (2008), pp. 1097–1112.

[23] Müller L. O., F. E. Fossan, A.T. Bråten, A. Jørgensen, R. Wiseth, and L. R. Hellevik. "Impact of baseline coronary flow and its distribution on fractional flow reserve prediction". In: *International journal for numerical methods in biomedical engineering* 37.11 (2019), e3246.

[24] World Health Organization. *Top 10 Causes of Death*. URL: `https://www.who.int/news-room/fact-sheets/detail/the-top-10-causes-of-death`. 2020.

[25] Mantero S., R. Pietrabissa, and R. Fumero. "The coronary bed and its role in the cardiovascular system: a review and an introductory single-branch model". In: *Journal of biomedical engineering* 14.2 (1992), pp. 109–116.

[26] Sakamoto S., S. Takahashi, A. U. Coskun, M. I. Papafaklis, A. Takahashi, S. Saito, P. H. Stone, and C. L. Feldman. "Relation of distribution of coronary blood flow volume to coronary artery dominance". In: *The American journal of cardiology* 111.10 (2013), pp. 1420–1424.

[27] Wu W., D. R. Pan, N. Foin, S. Pang, P. Ye, N. Holm, X. M. Ren, J. Luo, A. Nanjundappa, and S. L. Chen. "Noninvasive fractional flow reserve derived from coronary computed tomography angiography for identification of ischemic lesions: a systematic review and meta-analysis". In: *Scientific reports* 6.1 (2016), pp. 1–10.

[28] Huo Y. and G. S. Kassab. "Intraspecific scaling laws of vascular trees". In: *Journal of The Royal Society Interface* 9.66 (2012), pp. 190–200.

[29] Kim H. Y., H. S. Lim, J. H. Doh, C. W. Nam, E. S. Shin, B. K. Koo, M. H. Yoon, S. J. Tahk, D. K. Kang, Y. B. Song, et al. "Physiological severity of coronary artery stenosis depends on the amount of myocardial mass subtended by the coronary artery". In: *JACC: Cardiovascular Interventions* 9.15 (2016), pp. 1548–1560.

MOX Technical Reports, last issues

Dipartimento di Matematica
Politecnico di Milano, Via Bonardi 9 - 20133 Milano (Italy)

45/2022 Franco, N.; Fresca, S.; Manzoni, A.; Zunino, P.
Approximation bounds for convolutional neural networks in operator learning

44/2022 Peli, R.; Dovera, L.; Fighera, G.; Menafoglio, A.; Secchi, P.
Forecasting Oil Production Rates in Primary Depletion using the Physics-based Residual Kriging functional approach

43/2022 Zappon E.; Manzoni A.; Gervasio P.; Quarteroni A.
A reduced order model for domain decompositions with non-conforming interfaces

42/2022 Gatti, F.; Fois, M.; de Falco, C.; Perotto, S.; Formaggia, L.
Parallel simulations for fast-moving landslides: space-time mesh adaptation and sharp tracking of the wetting front

41/2022 Arnone, A.; Ferraccioli, F.; Pigolotti, C.; Sangalli, L.M.
A roughness penalty approach to estimate densities over two-dimensional manifolds

40/2022 Fumagalli, A.; Patacchini, F. S.
Well-posedness and variational numerical scheme for an adaptive model in highly heterogeneous porous media

39/2022 Ferro, N.; Perotto, S.; Gavazzoni, M.
A new fluid-based strategy for the connection of non-matching lattice materials

38/2022 Burzacchi, A.; Landrò, M.; Vantini, S.
Object-oriented Classification of Road Pavement Type in Greater Maputo from Satellite Images

37/2022 Boon, W. M.; Fumagalli, A.
A Reduced Basis Method for Darcy flow systems that ensures local mass conservation by using exact discrete complexes

35/2022 Perotto, S.; Bellini, G.; Ballarin, F.; Calò, K.; Mazzi, V.; Morbiducci, U.
Isogeometric hierarchical model reduction for advection-diffusion process simulation in microchannels